Published in final edited form as:
Amino Acids. 2012 July ; 43(1): 405–413. doi:10.1007/s00726-011-1096-7.

In vivo targeting of HER2-positive tumor using 2-helix affibody molecules

Gang Ren,
Molecular Imaging Program at Stanford (MIPS), Department of Radiology and Bio-X Program, Stanford University, California, Stanford, CA 94305-5344, USA

Jack M. Webster,
General Electric Company, Global Research Center, Niskayuna, NY 12309, USA

Zhe Liu,
Molecular Imaging Program at Stanford (MIPS), Department of Radiology and Bio-X Program, Stanford University, California, Stanford, CA 94305-5344, USA

Rong Zhang,
General Electric Company, Global Research Center, Niskayuna, NY 12309, USA

Zheng Miao,
Molecular Imaging Program at Stanford (MIPS), Department of Radiology and Bio-X Program, Stanford University, California, Stanford, CA 94305-5344, USA

Hongguang Liu,
Molecular Imaging Program at Stanford (MIPS), Department of Radiology and Bio-X Program, Stanford University, California, Stanford, CA 94305-5344, USA

Sanjiv S. Gambhir,
Molecular Imaging Program at Stanford (MIPS), Department of Radiology and Bio-X Program, Stanford University, California, Stanford, CA 94305-5344, USA

Faisal A. Syud, and
General Electric Company, Global Research Center, Niskayuna, NY 12309, USA

Zhen Cheng
Molecular Imaging Program at Stanford (MIPS), Department of Radiology and Bio-X Program, Stanford University, California, Stanford, CA 94305-5344, USA

Molecular Imaging Program at Stanford, Departments of Radiology, Stanford University, 1201 Welch Road, Lucas Expansion, P020A, Stanford, CA 94305, USA

Zhen Cheng: zcheng@stanford.edu

Abstract

Molecular imaging of human epidermal growth factor receptor type 2 (HER2) expression has drawn significant attention because of the unique role of the HER2 gene in diagnosis, therapy and

Correspondence to: Zhen Cheng, zcheng@stanford.edu.

prognosis of human breast cancer. In our previous research, a novel cyclic 2-helix small protein, MUT-DS, was discovered as an anti-HER2 Affibody analog with high affinity through rational protein design and engineering. MUT-DS was then evaluated for positron emission tomography (PET) of HER2-positive tumor by labeling with two radionuclides, ^{68}Ga and ^{18}F, with relatively short half-life ($t_{1/2}$ < 2 h). In order to fully study the in vivo behavior of 2-helix small protein and demonstrate that it could be a robust platform for labeling with a variety of radionuclides for different applications, in this study, MUT-DS was further radiolabeled with ^{64}Cu or ^{111}In and evaluated for in vivo targeting of HER2-positive tumor in mice. Design 1,4,7,10-tetraazacyclododecane- 1,4,7,10-tetraacetic acid (DOTA) conjugated MUT-DS (DOTA–MUT-DS) was chemically synthesized using solid phase peptide synthesizer and I_2 oxidation. DOTA–MUTDS was then radiolabeled with ^{64}Cu or ^{111}In to prepare the HER2 imaging probe (^{64}Cu/^{111}In-DOTA–MUT-DS). Both biodistribution and microPET imaging of the probe were evaluated in nude mice bearing subcutaneous HER2-positive SKOV3 tumors. DOTA–MUT-DS could be successfully synthesized and radiolabeled with ^{64}Cu or ^{111}In. Biodistribution study showed that tumor uptake value of ^{64}Cu or ^{111}In-labeled DOTA–MUT-DS was 4.66 ± 0.38 or 2.17 ± 0.15%ID/g, respectively, in nude mice bearing SKOV3 xenografts (n = 3) at 1 h post-injection (p.i.). Tumor-to-blood and tumor-to-muscle ratios for ^{64}Cu-DOTA-MUT-DS were attained to be 3.05 and 3.48 at 1 h p.i., respectively, while for ^{111}In-DOTA–MUT-DS, they were 2.04 and 3.19, respectively. Co-injection of the cold Affibody molecule $Z_{HER2:342}$ with ^{64}Cu-DOTA-MUT-DS specifically reduced the SKOV3 tumor uptake of the probe by 48%. ^{111}In-DOTA–MUT-DS displayed lower liver uptake at all the time points investigated and higher tumor to blood ratios at 4 and 20 h p.i., when compared with ^{64}Cu-DOTA–MUT-DS. This study demonstrates that the 2-helix protein based probes, ^{64}Cu/^{111}In DOTA–MUT-DS, are promising molecular probes for imaging HER2-positive tumor. Two-helix small protein scaffold holds great promise as a novel and robust platform for imaging and therapy applications.

Keywords

Affibody; HER2; PET; Molecular imaging; ^{111}In; ^{64}Cu

Introduction

The epidermal growth factor receptor (EGFR) family is a group of receptor tyrosine kinases (RTKs) which have been shown to be key regulators of many cellular events, making them important targets in cancer research (Ciardiello and Tortora 2008; Yarden and Shilo 2007). Of the four members of the EGFR family, human epidermal growth factor receptor type 2 (HER2) is a well-established tumor biomarker over-expressed in a wide variety of cancers including breast, ovarian, lung, gastric, oral and urogenital cancers (Glisson et al. 2004; Mitra et al. 1994; Swanton et al. 2006; Yeh et al. 1999; Engel and Kaklamani 2007; Nanda 2007). HER2-targeted therapy using Herceptin and/or combination with conventional therapeutic regimens has shown significant benefits in breast cancer patients (Harries and Smith 2002; Lazaridis et al. 2008; Tokuda et al. 2009). HER2 has great value as a molecular target for therapeutic intervention. Moreover, HER2 is an important prognostic indicator of cancer patients (Gravalos and Jimeno 2008; Ferretti et al. 2007; Serrano-Olvera et al. 2006).

Antibody-based radionuclide imaging has been extensively investigated to monitor HER2 status and relevance to therapy. Radiolabeled Herceptin has shown promise in noninvasive evaluation of HER2 expression in vivo (Niu et al. 2009; Tang et al. 2005; Dijkers et al. 2009; Smith-Jones et al. 2004). However, Herceptin is a large protein and may not be ideal for PET imaging because of its slow clearance and tumor-targeting ability. Affibody protein which binds to a different epitope on HER2 may be a more suitable imaging candidate for the purpose of in vivo monitoring of HER2 expression (Orlova et al. 2009; McLarty et al. 2009a). Additionally, Affibody proteinbased molecular imaging technology has shown great advantages over antibodies because of the short blood circulation and rapid and excellent tumor uptake of Affibody molecules (Tolmachev 2008). Affibody molecules are engineered non-immunogenic small proteins with 58-amino acid residues (~7 kDa) and a 3-helix bundle structure (Nygren 2008; Nygren and Skerra 2004; Tolmachev et al. 2007a). HER2-binding Affibody molecules with picomolar affinity have been identified and investigated as therapeutic and imaging agents for HER2-overexpressing malignant tumors (Orlova et al. 2009; McLarty et al. 2009b; Kramer-Marek et al. 2009; Wallberg et al. 2009; Tran et al. 2007; Tolmachev et al. 2006, 2009; Orlova et al. 2006; Cheng et al. 2008; Ahlgren et al. 2009). In our previous studies, we have found that of the various anti- HER2 Affibody protein constructs available (monomeric vs. dimeric), the smaller ones performed substantially better in vivo in terms of tumor uptake as well as better clearance (Cheng et al. 2008). Therefore, to make even smaller version of Affibody constructs, one α-helix (helix 3) that is not directly responsible for receptor recognition in the $Z_{HER2:342}$ was truncated, while preserving the binding domain that is composed of surface-exposed amino acid residues in the two α-helices (helix 1 and 2) bundles of Affibody (Fig. 1) (Webster et al. 2009). A library of such 2-helix protein constructs with ~4.6 kDa molecular weight (MW) was chemically synthesized and evaluated. Several disulfide bridge-constrained 2-helix constructs with high HER2 affinity [low nanomolar (nM)] were successfully identified (Webster et al. 2009).

The small size and high HER2-binding affinities of these 2-helix proteins encouraged us to further evaluate their potential use for in vivo molecular imaging of tumors. One cyclic 2-helix small protein with 5 nM HER2-binding affinity was then selected and conjugated with 1,4,7,10- tetraazacyclododecane-1,4,7,10-tetraacetic acid (DOTA) to obtain a bioconjugate DOTA-MUT-DS [sequence: VENK (homoC)NKEMR NRYWEAALDPNLNNQQKRAKIRSI YDDP(homoC)-NH_2, a disulfide bridge was formed between two homo-cysteine residues]. In previous research, PET radionuclides with relative short half-life, ^{68}Ga ($t_{1/2}$ = 67.7 min) and ^{18}F ($t_{1/2}$ = 109.8 min) were used to label MUT-DS for HER2 PET imaging (Ren et al. 2009; Miao et al. 2011). In order to fully study the in vivo behavior of 2-helix small protein and demonstrate that it could be a robust platform for labeling with a variety of radionuclides for different applications, in this study, MUT-DS was further radiolabeled with ($t_{1/2}$ = 12.7 h) or ^{111}In ($t_{1/2}$ = 2.8 d) and evaluated for in vivo targeting of HER2-positive tumor in mice.

Materials and methods

General

The anti-HER2 Affibody molecule $Z_{HER2:477}$ was purchased from Affibody AB (Bromma, Sweden). DOTA-tri-*tert*-butyl ester was obtained from Macrocyclics Inc. (Dallas, TX, USA). (S)-2-(Fmoc-amino)-4-tritylsulfanyl-butyric acid (Fmoc–HomoCys(Trt)-OH) was purchased from Bachem Bioscience, Inc (King of Prussia, PA, USA). All other N-α-Fmoc-protected amino acids were purchased from Advanced Chemtech (Louisville, KY, USA). Dimethylformamide (DMF) and methylene chloride were from Fisher Scientific (Fair Lawn, NJ, USA). Piperidine (20%) in DMF and 0.4 M of *N*-methylmorpholine (NMM) in DMF were from Protein Technologies Inc. (Tucson, AZ, USA). Trifluoroacetic acid (TFA), *O*-benzotriazole-*N*,*N*,*N*′,*N*′-tetramethyluronium hexafluorophosphate (HBTU), and 4-(2’,4’-dimethoxyphenyl-Fmoc-aminomethyl)-phenoxy resin (Rink amide resin LS, 100-200 mesh, 1% DVB, 0.2 mmol/g) were from Advanced Chemtech. Pyridine, acetic anhydride, acetic acid, and anhydrous ether were from J.T.Baker (Phillipsburg, NJ, USA). Triisopropylsilane (TIPS) and 1, 2-ethanedithiol (EDT) were purchased from Aldrich (Milwaukee, WI, USA). High-performance liquid chromatography (HPLC) grade acetonitrile (CH_3CN) and Millipore 18 mΩ water were used for peptide purifications. All other standard synthesis reagents were purchased from Sigma–Aldrich Chemical Co. (St. Louis, MO, USA). The radionuclide ^{111}In was purchased from Perkin Elmer (Waltham, MA, USA) while ^{64}Cu was provided by the Department of Medical Physics, University of Wisconsin at Madison (Madison, WI, USA). All the other general materials (cell lines, mice, etc.) and instruments (reverse phase HPLC, radioactive dose calibrator, Mass spectrometer) are the same as that previously reported (Cheng et al. 2008).

Synthesis of DOTA–MUT-DS

Synthesis of the cyclic 2-helix small protein, DOTA–MUT-DS, was the same as described in our previous reports (Webster et al. 2009). Briefly, peptide was synthesized using standard solid-phase peptide synthesizer (Fmoc chemistry). Then the linear peptide was cyclized by I_2 oxidation of the two homo-cysteines. Both crude linear and cyclic peptides were purified by a reversed-phase preparative HPLC with a protein and peptide C4 column (Vydac, Hesperia, CA, USA). The identity of the target peptides was confirmed by matrix-assisted laser desorption/ionization time of flight mass spectrometry (MALDI–TOF–MS, model: Perseptive Voyager-DE RP Biospectrometer) (Framingham, MA, USA) or an electrospray ionization time of flight mass spectrometer (ESI-TOF–MS, model: JMS-T100LC) (JEOL, Tokyo, Japan).

Radiochemistry

DOTA–MUT-DS was radiolabeled with ^{64}Cu or ^{111}In by addition of 111 MBq (3 mCi) $^{64}CuCl_2$ or $^{111}InCl_3$ (1 μg of peptide per 5.6 MBq radioactive material) in NaOAc (for ^{64}Cu) or NH_4OAc (for ^{111}In) buffer (0.1 N, pH 5.5) followed by a 40-min incubation at 40°C (for ^{64}Cu) or 80°C (for ^{111}In), respectively. The radiolabeled complex was then purified by a PD-10 column (GE Healthcare, Piscataway, NJ, USA). The product was washed out by phosphate-buffered saline (PBS) and passed through a 0.22 μm Millipore filter into a sterile vial for in vitro and animal experiments. Radioanalytical HPLC was used

to analyze the purified ^{64}Cu or ^{111}In-labeled-DOTA–MUT-DS. The flow rate was 1 mL/min, with the mobile phase starting from 95% solvent A (H_2O/0.1%TFA) and 5% solvent B (CH_3CN/0.1%TFA) (0–3 min) to 35% solvent A and 65% solvent B at 33 min, then going to 15% solvent A and 85% solvent B (33–36 min), maintaining this solvent composition for another 3 min (36–39 min) and returning to initial solvent composition by 42 min.

Serum stability

^{64}Cu/^{111}In-DOTA–MUT-DS (370 kBq) in 50 μL of PBS was added to 500 μL of mouse serum (Sigma, St. Louis, MO, USA). After incubation at 37°C for 1 h, the solution was analyzed by thin layer chromatography (TLC). The developing solution was 50% H_2O/50% CH_3CN.

SKOV3 tumor xenografts

SKOV3 cells were harvested and 3×10^6 cells were diluted in 100 μL of PBS then subcutaneously implanted into the right upper shoulder of 6- to 7-week-old female nu/nu mouse (Charles River, Wilmington, MA, USA). Tumors were allowed to grow to a size of 500–750 mg (2–3 weeks), and the tumor-bearing mice were subjected to in vivo biodistribution and imaging studies.

Biodistribution studies

SKOV3 tumor-bearing mice (n = 3 for each group) were injected with ^{64}Cu-DOTA–MUT-DS (0.69–1.01 MBq, 18.7–27.4 μCi, 0.58–0.86 μg) or ^{111}In-DOTA–MUT-DS (0.26–0.3 MBq, 7–8 μCi, 0.12 μg) through the tail vein and killed at 1, 4 and 20 h post-injection (p.i.). For a blocking study, another group of SKOV3 tumor-bearing mice (n = 3) were co-injected with 300 μg unlabeled $Z_{HER2:477}$ in PBS containing 2% bovine albumin serum (Invitrogen, Carlsbad, CA, USA) and killed at 4 h p.i. Tumor and normal tissues of interest were excised and weighed, and their radio activity was measured in a Wallac 1480 automated counter (Perkin Elmer, MA, USA). The radioactivity uptake in the tumor and normal tissues was expressed as a percentage of the injected radioactive dose per gram of tissue (% ID/g). The ratio of tumor to blood (T/B) and tumor to muscle (T/M) were determined based upon % ID/g.

MicroPET imaging

PET imaging of tumor-bearing mice was performed on a microPET R4 rodent model scanner (Concord Microsystem, Knoxville, TN). The mice bearing SKOV3 tumors were injected with ^{64}Cu-DOTA–MUT-DS (1 MBq, 27 μCi, 0.9 μg) via the tail vein. For another group of mice bearing SKOV3 tumors (n = 3), each mouse was coinjected with the same activity of probe and 300 μg of non-radiolabeled $Z_{HER2:477}$. At different times p.i. (0.5, 1, 2, 4 and 20 h), the mice were anesthetized with 2% isofluorane and placed in the prone position and the center of the filed of view of microPET. The 5-min static scans were obtained and the images were reconstructed by a two-dimensional ordered-subset expectation maximum (OSEM) algorithm.

Statistical methods

Statistical analysis was performed using the Student's *t* test for unpaired data. A 95% confidence level was chosen to determine the significance between groups, with $P < 0.05$ being significantly different.

Results

Chemistry and radiochemistry

DOTA–MUT-DS was successfully synthesized using standard peptide synthesis chemistry and I_2 oxidation ($[M + H]^+$, $C_{218}H_{352}N_{69}O_{69}S_3$, expected MW: 5136.77; measured: 5136.53). The synthetic yield for the 2-helix Affibody analog is usually ~10% with over 95% chemical purity. The peptide was then radiolabeled with ^{64}Cu or ^{111}In. The purification of radiolabeling solution, using a PD-10 column, afforded $^{64}Cu/^{111}In$-DOTA–MUT-DS with >95% radiochemical purity with modest specific activity 3.98–6.83 MBq/nmol (21–36 μCi/μg). HPLC analysis of ^{64}Cu-MUT-DS and ^{111}In-DOTA–MUT-DS both showed its retention time is 20 min. Further mouse serum stability study demonstrated that over 95% radiolabeled complex of $^{64}Cu/^{111}In$-DOTA–MUT-DS remained labeled product after 1 h incubation at 37°C.

Biodistribution studies

Biodistribution results for ^{64}Cu-DOTA–MUT-DS at 1, 4 and 20 h p.i. were summarized in Table 1. Rapid and high activity accumulation in the SKOV3 tumors was observed at early time points (4.66 ± 0.38%ID/g at 1 h p.i.). Tumor uptake slightly reduced to 3.34 ± 0.89%ID/g at 4 h; then the activity was slowly washed out from the tumor and reached 2.13 ± 1.11%ID/g over 20 h (Table 1). The blood uptake was 1.54 ± 0.18%ID/g at 1 h p.i., while it remained for 1.1 ± 0.02%ID/g at 20 h p.i. The tumor to blood ratio could attain around 3.05 ± 0.3 at 1 h p.i. and decreased over 20-h periods. While tumor to muscle ratio continued to increase from 3.48 ± 0.53 at 1 h p.i. to 5.56 ± 2.15 at 4 h p.i. Very high renal uptake and was found for the probe with 254.2 ± 19.1%ID/g at 1 h and the activity was washed out and reached 24.97 ± 8.03 at 20 h p.i. The liver uptake was 27.76 ± 6.4 and 13.39 ± 3.65%ID/g at 1 and 20 h p.i., respectively (Table 1). Specificity of the probe was then examined in a separate group of mice ($n = 3$); the co-injection of 300 μg of unlabeled $Z_{HER2:477}$ significantly reduced the tumor uptake from 3.34 ± 0.89 to 1.76 ± 0.12%ID/g at 4 h p.i. ($P < 0.05$), with 48.2% inhibition (Fig. 2). Though liver uptake also decreased from 20.25 ± 5.77 to 12.27 ± 2.2 while kidney uptake increased from 137.7 ± 17.3 to 214.2 ± 48.5 at 4 h p.i., they were not significantly different compared with nonblocking group ($P > 0.05$) (Table 1).

Interestingly, in vivo biodistribution of ^{111}In-DOTA–MUT-DS showed some difference from the ^{64}Cu-labeled one (Table 2). The tumor uptake reached comparable level as that of ^{64}Cu-DOTA–MUT-DS, but the blood clearance was faster (1.06 ± 0.13%ID/g at 1 h while only 0.18 ± 0.02%ID/g at 20 h p.i.) when compared with ^{64}Cu-DOTA–MUT-DS. Thus the tumor to blood ratio for ^{111}In- DOTA–MUT-DS reached 9.57 ± 0.93 at 20 h p.i. Both the liver and intestine uptakes for ^{111}In-DOTA–MUT-DS were significantly lower than that of ^{64}Cu-DOTA–MUT-DS at all time points ($P < 0.05$).

MicroPET imaging

Decay-corrected coronal microPET images of a mouse bearing SKOV3 tumor at 0.5, 1, 2, 4 and 20 h and a mouse injected with the probe and unlabeled $Z_{HER2:477}$ are shown in Figs. 3, 4, respectively. For ^{64}Cu-DOTA–MUT-DS, SKOV3 tumor was clearly visualized with good tumor-tobackground contrast from 0.5 to 20 h p.i. Liver activity was observable while high activity accumulation was particularly obvious in the kidney region, which was consistent with the findings from the biodistribution study. Furthermore, the co-injection of unlabeled Affibody $Z_{HER2:477}$ significantly reduced the uptake of ^{64}Cu-DOTA–MUT-DS in the tumor, resulting in a much lower tumor to background contrast in vivo (Fig. 4).

Discussion

A variety of radiolabeled Affibody molecules have been successfully demonstrated to be promising molecular probes for imaging HER2 expression in living subjects (Orlova et al. 2006, 2009; McLarty et al. 2009). ^{18}F-labeled 3-helix Affibody dimer $(Z_{HER2:477})_2$ and monomer $Z_{HER2:477}$ were recently evaluated in tumor-bearing mice by our group (Tolmachev et al. 2007). It was found that monomer showed much better in vivo pharmacokinetics such as higher tumor uptake and faster blood clearance than that of dimer, though it had lower in vitro HER2 binding affinity (Nygren and Skerra 2004). In this research, a cyclic 2-helix Affibody analog MUT-DS was selected for DOTA conjugation, radiolabeling with radiometals (^{64}Cu or ^{111}In) with longer half-life and microPET imaging. The potential advantages expected for smaller protein constructs include easy library generation for screening, economic viability, potentially low immunogenic potential, high specific tumor-targeting ability, fast tumor extravasation, and reasonable tumor accumulation and retention.

Biodistribution studies of ^{64}Cu or ^{111}In-labeled DOTA–MUT-DS were then performed to evaluate the in vivo behavior of the 2-helix small protein. Considering the relatively longer half-life of ^{64}Cu (12.7 h) compared with other PET probes such as ^{68}Ga or ^{18}F, this study provides us more comprehensive profiles of the in vivo behaviors of ^{64}Cu-DOTA–MUT-DS. ^{111}In has an even longer half-life of 68 h and has been extensively utilized as a surrogate isotope for ^{90}Y or ^{177}Lu, both of which are suitable for radionuclide therapy (Ellisonet al. (2010); McDevitt et al. 2007). With all these radiolabels, we may comprehensively evaluate 2-helix small protein as a novel platform for in vivo targeted imaging of HER2 expression.

It was found that 2-helix probes still preserved good in vivo tumor-targeting ability. The ^{64}Cu-DOTA–MUT-DS displayed 4.66 ± 0.38, 3.34 ± 0.89 and 2.13 ± 1.13%ID/g SKOV3 tumor uptake at 1, 4 and 20 h, respectively (Table 1). The slightly higher tumor uptake at 1 h than that of 4 h suggests the rapid tumor-targeting ability of 2-helix probe, likely due to the small size of the protein. Meanwhile, compared with tumor uptake at 1 h, 46% of radioactivity still remained in tumor at 20 h p.i., indicating good tumor retention for ^{64}Cu-DOTA–MUT-DS. Furthermore, the success of inhibition of the probe tumor uptake using the cold Affibody molecule $Z_{HER2:477}$ (3.34 ± 0.89 vs. 1.76 ± 0.12%ID/g, 4 h p.i., $P < 0.05$) proved the in vivo tumor-targeting specificity of the probe (Fig. 2). In addition, reasonable tumor-to-blood and tumor-muscle ratios (3.05 and 3.48) were attained at 1 h p.i.,

suggesting ^{64}Cu-DOTA–MUT-DS can be used for tumor imaging. Lower tumor-to-blood ratio (1.36) was achieved at 20 h, mainly because of the relatively high activity residue in the blood. But good tumor-to-muscle ratio (3.72) at 20 h still warrants the good tumor imaging quality (Fig. 3). High uptake in liver and moderate uptake in intestines were also observed, indicating that the probe was partially cleared through hepatobiliary system. This is also caused by the low in vivo stability of ^{64}Cu–DOTA complex (Boswell et al. 2004). The in vivo tumor imaging ability of ^{64}Cu-DOTA–MUT-DS was further examined using SKOV3 tumor mice and microPET imaging. Excellent tumor to background contrast was obtained as early as 30 min after intravenous injection of the probe (Fig. 4), confirming the fast tumor targeting and clearance of the 2-helix protein. Good tumor localization and contrast were also observed at 20 h p.i.; consistent with the finding obtained in biodistribution study. Similarly, SKOV3 tumors were not visible in the mice with co-injection of cold Affibody molecules (Fig. 4), suggesting good specificity of the probe in vivo.

DOTA is the most commonly used chelator for radiometal labeling. However, considering of some potential limitations of using DOTA as chelators for ^{64}Cu labeling, we also used ^{111}In to label the small protein and tested the biodistribution of ^{111}In-DOTA–MUT-DS (Boswell et al. 2004; Prasanphanich et al. 2007). Different from what we observed for ^{64}Cu-DOTA–MUT-DS, ^{111}In-DOTA–MUTDS showed much lower liver and intestine uptakes in vivo. This is likely resulted from the higher stability of ^{111}Inlabeled peptides. When compared with ^{64}Cu-DOTA– MUT-DS, the blood clearance of ^{111}In-DOTA–MUT-DS was faster; thus, a higher tumor to blood ratios could be attained at later time points. For example, the tumor to blood ratio for ^{111}In-DOTA–MUT-DS was about 9.57 at 20 h, which ensures the feasibilities of using ^{111}In-DOTA–MUT-DS for single photon emission computed tomography (SPECT) imaging of HER2 expression in vivo.

^{111}In is a surrogate radionuclide for beta emitter ^{90}Y as well as emits both therapeutic Auger and internal conversion electrons (Capello et al. 2003); thus, radionuclide therapeutic potential of MUT-DS could also be evaluated when using ^{111}In as a radiolabel. In this study, the ^{111}In-labeled MUT-DS shows good tumor uptakes and retention; thus, it does have potential for HER2-targeted radionuclide therapies. Some other strategies such as including a human serum albumin (HSA)-binding domain or HSA itself to 2-helix protein were also under investigation to optimize the radiocomplexes for radionuclide therapy purpose (Andersen et al. 2011; Tolmachev et al. 2007b).

Many reports have demonstrated that radiometal-labeled 3-helix Affibody molecules displayed high kidney uptake and retention, which may limit their applications for tumor imaging and treatment, especially when Affibody is labeled with therapeutic radionuclides (Tolmachev et al. 2006, 2007b; Wallberg and Orlova 2008; Ekblad et al. 2008). Very high kidney uptake was also observed for ^{64}Cu or ^{111}In-DOTA–MUT-DS. The extremely high kidney uptake value for both radioconjugates suggested that the clearance of the radiometal-labeled 2-helix protein is mainly through kidney-urinary system. Our results indicate that the problem caused by high kidney uptake of Affibody protein could not be alleviated by simply reducing the size of the protein through truncating one alpha-helix (SANLLAEAKKLNDAQAPK). It is most likely that the amino acid residues presenting in

the helix 1 and 2 of the Affibody (Fig. 1) and the DOTA chelator contribute to the high kidney uptake of radiometal-labeled Affibody molecules. More studies are needed to understand the mechanism of the globular filtration and tubular reabsorption towards this particular class of proteins, in order to further optimize the probe for clinical translation. Several strategies established in the peptide/antibody-based imaging field may also be explored to reduce the high kidney uptake. First, different amino acid sequences, linker systems and chelators can be used to modulate the surface charge, lipophilicity and binding affinity of the protein; second, co-injection of cold amino acids such as lysine; and third, nonresidulized radioisotopes such as radiohalogens can also be used (Tolmachev et al. 2007b; Ekblad et al. 2008; Gotthardt et al. 2007).

Conclusion

A 2-helix Affibody analog has been successfully synthesized. Radiolabeled 2-helix small protein shows good in vitro stability and in vivo tumor-targeting ability. Biodistribution and microPET imaging studies further demonstrate that $^{64}Cu/^{111}In$-labeled 2-helix DOTA–MUT-DS are promising molecular probes for imaging HER2-positive tumor in living mice. Strategies to further optimize the biodistribution of the 2-helix proteins and 2-helix molecules against other targets are also under active investigation in our laboratories. Overall, the 2-helix small protein scaffold holds great promise as a novel platform that will likely be used for many imaging and therapy applications.

Acknowledgments

This work was supported, in part, by California Breast Cancer Research Program 14IB-0091 (ZC) and SNM Pilot Research Grant (ZC), Medical Diagnostics, GE Healthcare, and National Cancer Institute (NCI) Small Animal Imaging Resource Program (SAIRP) grant R24 CA93862. We also thank Dr. Joshua Hoerner, Gregory Goddard and Hans Grade of GE Global Research for MS analysis and Dr. Alex Gibson of GE Healthcare for their helpful suggestion and reviewing of the manuscript.

References

Ahlgren S, Wallberg H, Tran TA, Widstrom C, Hjertman M, Abrahmsen L, et al. Targeting of HER2-expressing tumors with a site-specifically 99mTc-labeled recombinant affibody molecule, ZHER2:2395, with C-terminally engineered cysteine. J Nucl Med. 2009; 50:781–789. [PubMed: 19372467]

Andersen JT, Pehrson R, Tolmachev V, Bekele MD, Abrahmsen L, Ekblad C. Extending half-life by indirect targeting of the neonatal Fc receptor (FcRn) using a minimal albumin binding domain (ABD). J Biol Chem. 2011

Boswell CA, Sun X, Niu W, Weisman GR, Wong EH, Rheingold AL, et al. Comparative in vivo stability of copper-64-labeled cross-bridged and conventional tetraazamacrocyclic complexes. J Med Chem. 2004; 47:1465–1474. [PubMed: 14998334]

Capello A, Krenning EP, Breeman WA, Bernard BF, de Jong M. Peptide receptor radionuclide therapy in vitro using [111In-DTPA0]octreotide. J Nucl Med. 2003; 44:98–104. [PubMed: 12515882]

Cheng Z, De Jesus O, Namavari M, De A, Levi J, Webster J, et al. Small-animal PET imaging of human epidermal growth factor receptor type 2 expression with site-specific ^{18}F-labeled protein scaffold molecules. J Nucl Med. 2008; 49:804–813. [PubMed: 18413392]

Ciardiello F, Tortora G. EGFR antagonists in cancer treatment. N Engl J Med. 2008; 358:1160–1174. [PubMed: 18337605]

Dijkers EC, Kosterink JG, Rademaker AP, Perk LR, van Dongen GA, Bart J, et al. Development and characterization of clinicalgrade 89Zr-trastuzumab for HER2/neu immunoPET imaging. J Nucl Med. 2009; 50:974–981. [PubMed: 19443585]

Ekblad T, Tran T, Orlova A, Widstrom C, Feldwisch J, Abrahmsen L, et al. Development and preclinical characterisation of 99mTc-labelled Affibody molecules with reduced renal uptake. Eur J Nucl Med Mol Imaging. 2008; 35:2245–2255. [PubMed: 18594815]

Ellison D, Kaufman J, Mather SJ. Automated radiolabelling of monoclonal antibodies with the Modular Lab system. Nucl Med Commun. 2010; 31:173–177. [PubMed: 19952855]

Engel RH, Kaklamani VG. HER2-positive breast cancer: current and future treatment strategies. Drugs. 2007; 67:1329–1341. [PubMed: 17547474]

Ferretti G, Felici A, Papaldo P, Fabi A, Cognetti F. HER2/neu role in breast cancer: from a prognostic foe to a predictive friend. Curr Opin Obstet Gynecol. 2007; 19:56–62. [PubMed: 17218853]

Glisson B, Colevas AD, Haddad R, Krane J, El-Naggar A, Kies M, et al. HER2 expression in salivary gland carcinomas: dependence on histological subtype. Clin Cancer Res. 2004; 10:944–946. [PubMed: 14871971]

Gotthardt M, van Eerd-Vismale J, Oyen WJ, de Jong M, Zhang H, Rolleman E, et al. Indication for different mechanisms of kidney uptake of radiolabeled peptides. J Nucl Med. 2007; 48:596–601. [PubMed: 17401097]

Gravalos C, Jimeno A. HER2 in gastric cancer: a new prognostic factor and a novel therapeutic target. Ann Oncol. 2008; 19:1523–1529. [PubMed: 18441328]

Harries M, Smith I. The development and clinical use of trastuzumab (Herceptin). Endocr Relat Cancer. 2002; 9:75–85. [PubMed: 12121832]

Kramer-Marek G, Kiesewetter DO, Capala J. Changes in HER2 expression in breast cancer xenografts after therapy can be quantified using PET and (18)F-labeled affibody molecules. J Nucl Med. 2009; 50:1131–1139. [PubMed: 19525458]

Lazaridis G, Pentheroudakis G, Pavlidis N. Integrating trastuzumab in the neoadjuvant treatment of primary breast cancer: accumulating evidence of efficacy, synergy and safety. Crit Rev Oncol Hematol. 2008; 66:31–41. [PubMed: 17766143]

McDevitt MR, Chattopadhyay D, Jaggi JS, Finn RD, Zanzonico PB, Villa C, et al. PET imaging of soluble yttrium-86-labeled carbon nanotubes in mice. PLoS One. 2007; 2:e907. [PubMed: 17878942]

McLarty K, Cornelissen B, Cai Z, Scollard DA, Costantini DL, Done SJ, et al. Micro-SPECT/CT with 111In-DTPA-pertuzumab sensitively detects trastuzumab-mediated HER2 downregulation and tumor response in athymic mice bearing MDA-MB-361 human breast cancer xenografts. J Nucl Med. 2009

McLarty K, Cornelissen B, Cai Z, Scollard DA, Costantini DL, Done SJ, et al. Micro-SPECT/CT with 111In-DTPApertuzumab sensitively detects trastuzumab-mediated HER2 downregulation and tumor response in athymic mice bearing MDA-MB-361 human breast cancer xenografts. J Nucl Med. 2009b; 50:1340–1348. [PubMed: 19617342]

Miao Z, Ren G, Liu H, Jiang L, Webster JM, Zhang R, et al. A Novel 18F-Labeled 2-Helix Small Protein for PET Imaging of HER2 Positive Tumor. Eur J Nucl Med Mol Imaging (Submitted). 2011

Mitra AB, Murty VV, Pratap M, Sodhani P, Chaganti RS. ERBB2 (HER2/neu) oncogene is frequently amplified in squamous cell carcinoma of the uterine cervix. Cancer Res. 1994; 54:637–639. [PubMed: 7905784]

Nanda R. Targeting the human epidermal growth factor receptor 2 (HER2) in the treatment of breast cancer: recent advances and future directions. Rev Recent Clin Trials. 2007; 2:111–116. [PubMed: 18473995]

Niu G, Li Z, Cao Q, Chen X. Monitoring therapeutic response of human ovarian cancer to 17-DMAG by noninvasive PET imaging with (64)Cu-DOTA-trastuzumab. Eur J Nucl Med Mol Imaging. 2009; 36:1510–1519. [PubMed: 19440708]

Nygren PA. Alternative binding proteins: affibody binding proteins developed from a small three-helix bundle scaffold. Febs J. 2008; 275:2668–2676. [PubMed: 18435759]

Nygren PA, Skerra A. Binding proteins from alternative scaffolds. J Immunol Methods. 2004; 290:3–28. [PubMed: 15261569]

Orlova A, Magnusson M, Eriksson T, Nilsson M, Larsson B, Hoiden-Guthenberg I, et al. Tumor imaging using a picomolar affinity HER2 binding affibody molecule. Cancer Res. 2006; 66:4339–4348. [PubMed: 16618759]

Orlova A, Wallberg H, Stone-Elander S, Tolmachev V. On the selection of a tracer for PET imaging of HER2-expressing tumors: direct comparison of a 124I-labeled affibody molecule and trastuzumab in a murine xenograft model. J Nucl Med. 2009; 50:417–425. [PubMed: 19223403]

Prasanphanich AF, Nanda PK, Rold TL, Ma L, Lewis MR, Garrison JC, et al. [64Cu-NOTA-8-Aoc-BBN(7–14)NH2] targeting vector for positron-emission tomography imaging of gastrinreleasing peptide receptor-expressing tissues. Proc Natl Acad Sci USA. 2007; 104:12462–12467. [PubMed: 17626788]

Ren G, Zhang R, Liu Z, Webster JM, Miao Z, Gambhir SS, et al. A 2-helix small protein labeled with 68 Ga for PET imaging of HER2 expression. J Nucl Med. 2009; 50:1492–1499. [PubMed: 19690041]

Serrano-Olvera A, Duenas-Gonzalez A, Gallardo-Rincon D, Candelaria M, De la Garza-Salazar J. Prognostic, predictive and therapeutic implications of HER2 in invasive epithelial ovarian cancer. Cancer Treat Rev. 2006; 32:180–190. [PubMed: 16483720]

Smith-Jones P, Solit D, Akhurst T, Afroze F, Rosen N, Larson S. Imaging the pharmacodynamics of HER2 degradation in response to Hsp90 inhibitors. Nat Biotechnol. 2004; 22:701–706. [PubMed: 15133471]

Swanton C, Futreal A, Eisen T. Her2-targeted therapies in nonsmall cell lung cancer. Clin Cancer Res. 2006; 12:4377s–4383s. [PubMed: 16857814]

Tang Y, Wang J, Scollard D, Mondal H, Holloway C, Kahn H, et al. Imaging of HER2/neu-positive BT-474 human breast cancer xenografts in athymic mice using $^{(111)}$In-trastuzumab (Herceptin) Fab fragments. Nucl Med Biol. 2005; 32:51–58. [PubMed: 15691661]

Tokuda Y, Suzuki Y, Saito Y, Umemura S. The role of trastuzumab in the management of HER2-positive metastatic breast cancer: an updated review. Breast Cancer. 2009

Tolmachev V. Imaging of HER-2 overexpression in tumors for guiding therapy. Curr Pharm Des. 2008; 14:2999–3019. [PubMed: 18991715]

Tolmachev V, Nilsson F, Widstrom C, Andersson K, Rosik D, Gedda L, et al. ^{111}In-benzyl-DTPA-$Z_{HER2:342}$, an affibody-based conjugate for in vivo imaging of HER2 expression in malignant tumors. J Nucl Med. 2006; 47:846–853. [PubMed: 16644755]

Tolmachev V, Orlova A, Nilsson FY, Feldwisch J, Wennborg A, Abrahmsen L. Affibody molecules: potential for in vivo imaging of molecular targets for cancer therapy. Expert Opin Biol Ther. 2007a; 7:555–568. [PubMed: 17373906]

Tolmachev V, Orlova A, Pehrson R, Galli J, Baastrup B, Andersson K, et al. Radionuclide therapy of HER2-positive microxenografts using a ^{177}Lu-labeled HER2-specific Affibody molecule. Cancer Res. 2007b; 67:2773–2782. [PubMed: 17363599]

Tolmachev V, Friedman M, Sandstrom M, Eriksson T, Rosik D, Hodik M, et al. Affibody Molecules for Epidermal Growth Factor Receptor Targeting In Vivo: Aspects of Dimerization and Labeling Chemistry. J Nucl Med. 2009; 50:274–283. [PubMed: 19164241]

Tran T, Engfeldt T, Orlova A, Sandstrom M, Feldwisch J, Abrahmsen L, et al. ^{99m}Tc-maEEE-$Z_{HER2:342}$, an Affibody moleculebased tracer for the detection of HER2 expression in malignant tumors. Bioconjug Chem. 2007; 18:1956–1964. [PubMed: 17944527]

Wallberg H, Orlova A. Slow internalization of anti-HER2 synthetic affibody monomer ^{111}In-DOTA-$Z_{HER2:342-pep2}$: implications for development of labeled tracers. Cancer Biother Radiopharm. 2008; 23:435–442. [PubMed: 18771347]

Wallberg H, Ahlgren S, Widstrom C, Orlova A. Evaluation of the radiocobalt-labeled [MMA-DOTA-Cys61]-Z HER2:2395 (-Cys) affibody molecule for targeting of HER2-expressing tumors. Mol Imaging Biol. 2009; 12:54–62. [PubMed: 19557480]

Webster JM, Zhang R, Gambhir SS, Cheng Z, Syud FA. Engineered two-helix small proteins for molecular recognition. Chembiochem. 2009; 10:1293–1296. [PubMed: 19422008]

Yarden Y, Shilo BZ. SnapShot: EGFR signaling pathway. Cell. 2007; 131:1018. [PubMed: 18045542]

Yeh S, Lin HK, Kang HY, Thin TH, Lin MF, Chang C. From HER2/Neu signal cascade to androgen receptor and its coactivators: a novel pathway by induction of androgen target genes through MAP kinase in prostate cancer cells. Proc Natl Acad Sci USA. 1999; 96:5458–5463. [PubMed: 10318905]

Abbreviations

DOTA	1,4,7,10-tetraazacyclododecane-1,4,7,10-tetraacetic acid
PET	Positron emission tomography
SPECT	Single photon emission computed tomography
HPLC	High-performance liquid chromatography
p.i.	Postinjection
MW	Molecular weight
OSEM	Ordered subsets expectation maximum

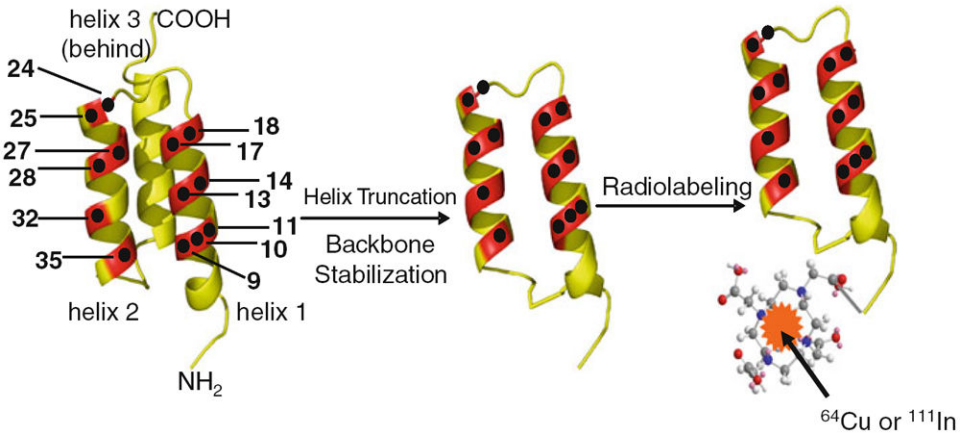

Fig. 1.

3-Helix Affibody and 2-helix protein scaffold-based PET probes for HER2 imaging. The *black dots* indicate the amino acid residues responsible for receptor binding

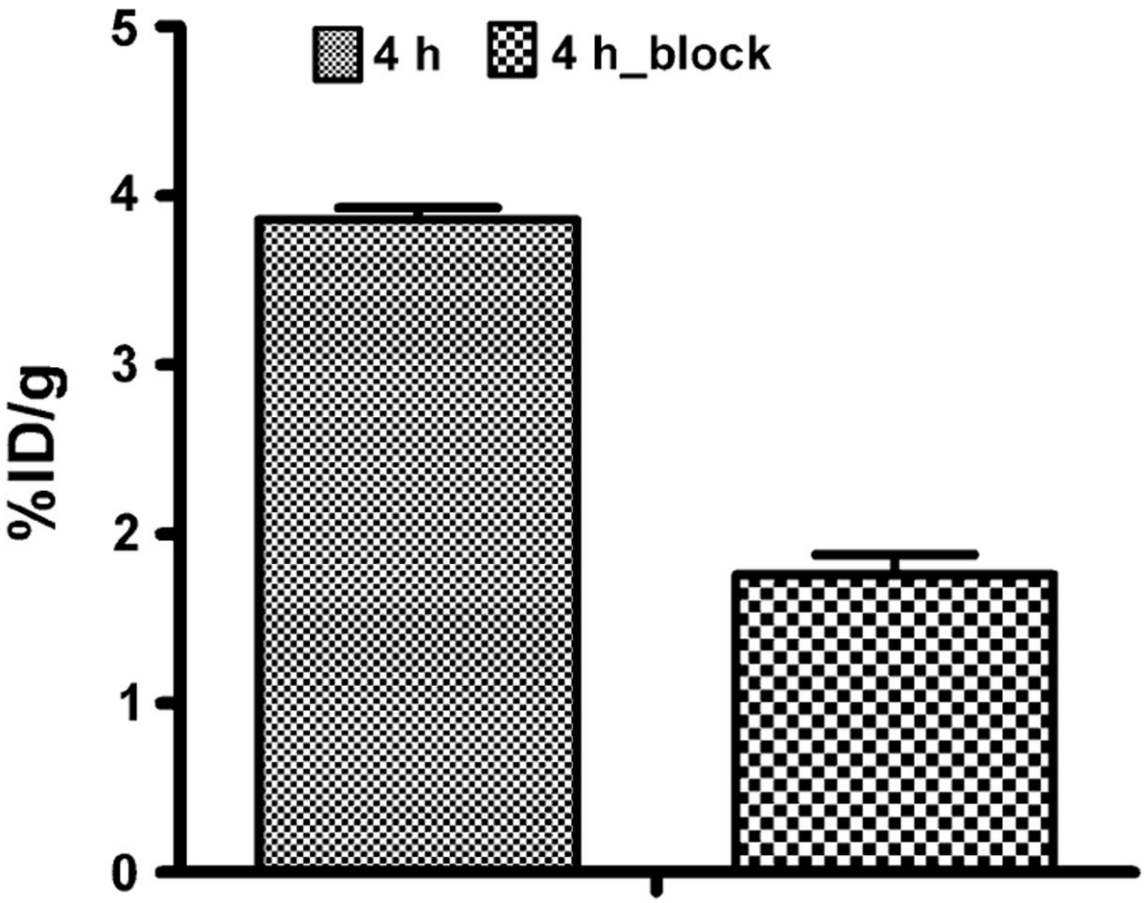

Fig. 2.

Tumor uptakes after co-injection of 300 μg of unlabeled $Z_{HER2:477}$ at 4 h p.i. Tumor uptake was blocked by 48.2%. Data were expressed as the percentage administered activity (injected dose) per gram of tissue (%ID/g) after intravenous injection of ^{64}Cu-DOTA–MUT-DS at 4 h p.i. (*n* = 3 for each group)

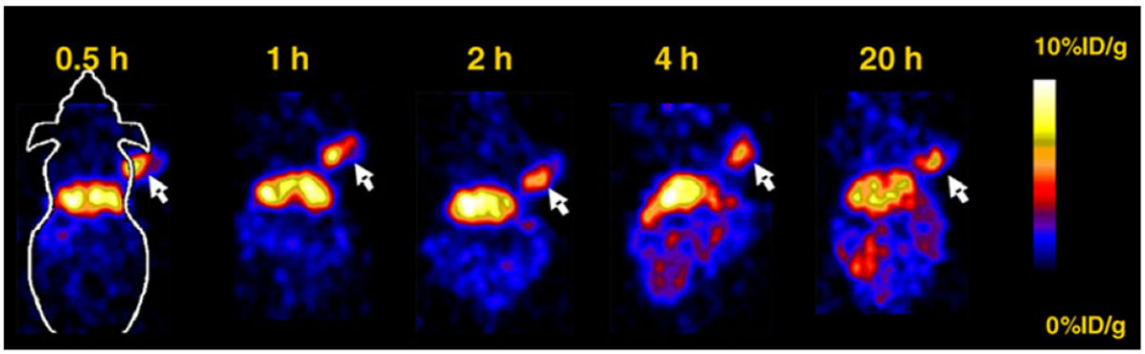

Fig. 3.

Decay-corrected coronal microPET images of a nude mouse bearing SKOV3 (indicated by *white arrows*) at 0.5, 1, 2, 4 and 20 h after tail vein injection of ^{64}Cu-DOTA–MUT-DS

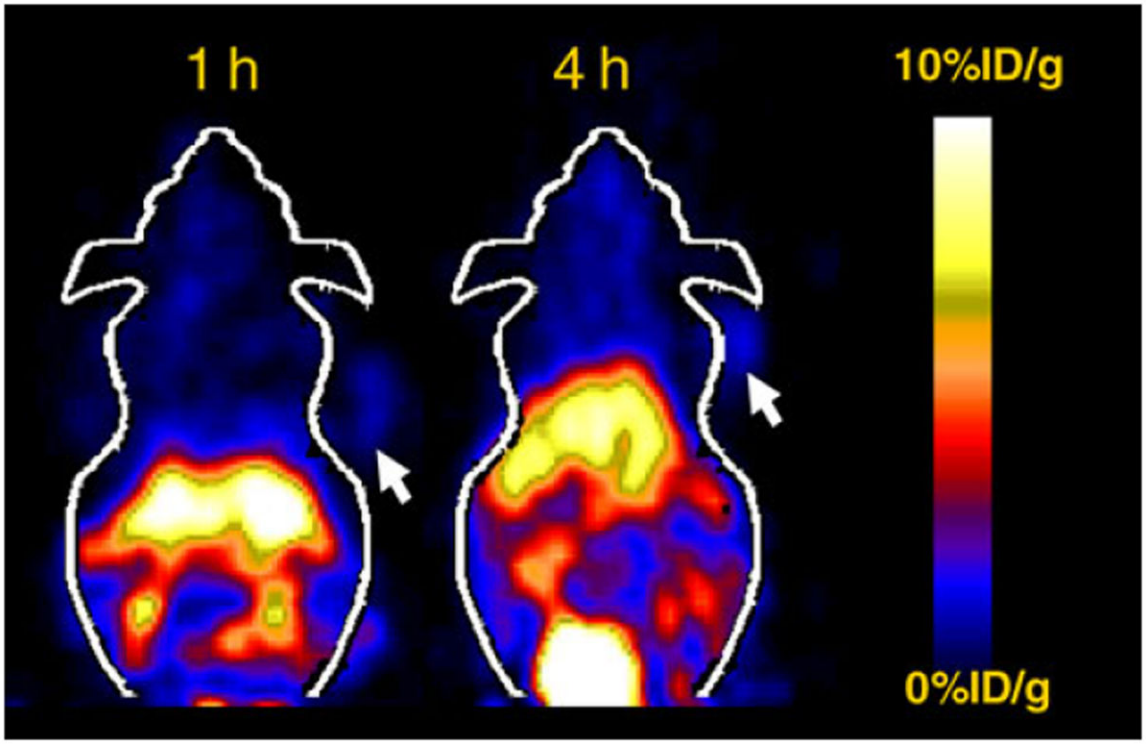

Fig. 4.

Decay-corrected coronal microPET images of a nude mouse bearing SKOV3 which was co-injected with $Z_{HER2:477}$ (300 μg) at 1 and 4 h p.i

Table 1

Biodistribution data for 2-helix ^{64}Cu-DOTA–MUTDS with or without co-injection of large excess of unlabeled $Z_{HER2:477}$ in nude mice bearing subcutaneously xenotransplanted SKOV3 human ovarian cancer

Organ (%ID/g)	1 h	4 h	4 h block	20 h
Tumor	4.66 ± 0.38	3.34 ± 0.89*	1.76 ± 0.12	2.13 ± 1.11
Blood	1.54 ± 0.18	1.74 ± 0.54	1.34 ± 0.30	1.10 ± 0.02
Heart	1.95 ± 0.19	1.98 ± 0.26	2.05 ± 0.40	2.23 ± 0.69
Liver	27.76 ± 6.4	20.25 ± 5.77	12.27 ± 2.19	13.39 ± 3.65
Lung	4.90 ± 1.28	3.56 ± 1.04	5.49 ± 1.20	2.92 ± 0.55
Muscle	1.35 ± 0.09	0.63 ± 0.11	0.75 ± 0.12	0.62 ± 0.27
Spleen	9.12 ± 0.98	2.73 ± 0.80	2.65 ± 0.74	2.81 ± 1.30
Brain	0.34 ± 0.11	0.22 ± 0.07	0.30 ± 0.07	0.28 ± 0.14
Intestine	4.46 ± 0.82	3.60 ± 1.30	3.42 ± 1.47	2.93 ± 0.82
Skin	1.36 ± 0.28	1.06 ± 0.21	1.40 ± 0.37	1.10 ± 0.28
Stomach	3.46 ± 1.24	3.37 ± 1.31	3.00 ± 0.44	2.50 ± 1.42
Pancreas	1.41 ± 0.40	1.47 ± 0.66	0.44 ± 0.20	0.92 ± 0.04
Bone	0.99 ± 0.34	0.62 ± 0.18	0.85 ± 0.13	0.67 ± 0.13
Kidney	254.2 ± 19.10	137.69 ± 17.27	214.18 ± 48.52	24.97 ± 8.03
Uptake ratio				
Tumor/Blood	3.05 ± 0.30	2.14 ± 1.05	1.36 ± 0.35	1.36 ± 0.04
Tumor/Muscle	3.48 ± 0.53	5.56 ± 2.15	2.39 ± 0.51	3.72 ± 1.65

Data are expressed as the percentage administered activity (injected dose) per gram of tissue (%ID/g) after intravenous injection of 0.69–1.01 MBq (18.7–27.4 μCi) probe at 1, 4, and 20 h p.i. (n = 3)

*P < 0.05, compared with 4 h block

Table 2

Biodistribution data for 2-helix ^{111}In-DOTA–MUTDS in nude mice bearing subcutaneously xenotransplanted SKOV3 human ovarian cancer

Organ (%ID/g)	1 h	4 h	20 h
Tumor	2.17 ± 0.51	3.41 ± 1.80	1.72 ± 0.22
Blood	1.06 ± 0.13	0.60 ± 0.06	0.18 ± 0.02
Heart	0.46 ± 0.11	0.41 ± 0.10	0.24 ± 0.08
Liver	10.24 ± 1.74	11.35 ± 1.54	8.69 ± 1.44
Lung	1.95 ± 0.67	1.21 ± 0.10	0.73 ± 0.25
Muscle	0.75 ± 0.25	0.69 ± 0.17	0.57 ± 0.15
Spleen	6.49 ± 1.17	5.10 ± 0.17	4.06 ± 0.09
Brain	0.14 ± 0.02	0.12 ± 0.01	0.10 ± 0.02
Intestine	0.36 ± 0.06	0.34 ± 0.04	0.48 ± 0.20
Skin	0.37 ± 0.14	0.38 ± 0.03	0.33 ± 0.06
Stomach	0.25 ± 0.05	0.25 ± 0.02	0.22 ± 0.05
Pancreas	0.28 ± 0.10	0.19 ± 0.02	0.20 ± 0.06
Bone	0.53 ± 0.19	0.39 ± 0.08	0.29 ± 0.05
Kidney	212.00 ± 48.23	254.67 ± 63.55	210.02 ± 31.95
Uptake ratio			
Tumor/Blood	2.04 ± 0.39	5.82 ± 2.56	9.57 ± 0.93
Tumor/Muscle	3.19 ± 1.45	4.45 ± 3.16	3.18 ± 0.78

Data are expressed as the percentage administered activity (injected dose) per gram of tissue (%ID/g) after intravenous injection of 0.26–0.3 MBq (7–8 μCi) probe at 1, 4, and 20 h p.i. (n = 3)